Decay of ^{6}Be populated in the ^{6}Li(^{3}He,^{3}H) charge-exchange reaction

P. Papka,[1,*] R. Álvarez-Rodríguez,[3,†] F. Nemulodi,[1] R. A. Bark,[1] S. P. Fox,[4] J. Gál,[2] T. T. Ibrahim,[5,‡] G. Kalinka,[2] N. Y. Kheswa,[1] E. A. Lawrie,[1] J. J. Lawrie,[1] E. O. Lieder,[1] R. M. Lieder,[1] T. E. Madiba,[1] J. Molnár,[2] S. M. Mullins,[1] R. T. Newman,[1] B. M. Nyakó,[2] O. Shirinda,[1] T. D. Singo,[1] and J. Timár[2]

[1]*iThemba LABS, Post Office Box 722, Somerset West 7129, South Africa*

[2]*Institute of Nuclear Research (ATOMKI), Post Office Box 51, H-4001 Debrecen, Hungary*

[3]*Department of Physics and Astronomy, University of Aarhus, DK-8000 Aarhus C, Denmark*

[4]*Department of Physics, University of York, York YO10 5DD, United Kingdom*

[5]*Department of Physics, University of Ilorin, PMB 1515, Ilorin, Nigeria*

(Received 20 August 2009; revised manuscript received 10 February 2010; published 18 May 2010)

A complete kinematic measurement of the ^{6}Li(^{3}He,^{3}H)αpp reaction is performed at $E_{\rm lab} = 50$ MeV, to investigate the cluster structure of ^{6}Be. The energy and angular distributions of the breakup particles, emitted from the ground and first excited states of ^{6}Be, are compared to three-body resonance and two-body sequential decay calculations. The results indicate a rather pure three-body configuration of the 2^{+} state of ^{6}Be but they are not conclusive regarding the decay mode of the 0^{+} state. No branching ratio between sequential and three-body decay paths could be extracted. Excitations above the 2^{+} state were populated at $E_{x} = 1.67$–23 MeV. Decay through ^{5}Li-p and ^{2}He-^{4}He channels is identified in the continuum of ^{6}Be, and the reaction mechanism is discussed.

DOI: 10.1103/PhysRevC.81.054308 PACS number(s): 25.60.Gc, 21.10.−k, 27.20.+n

I. INTRODUCTION

Decay-mode characterization of Borromean nuclei can be a very complex task, especially when parent and daughter resonances are broad. Beryllium-6 is a typical case where two two-body configurations, ^{2}He-^{4}He and ^{5}Li-p, are characterized by broad ^{2}He and ^{5}Li resonant ground states. The decay of states just below or near the threshold are characterized by continuous relative energy distributions, as illustrated in Fig. 1, and owing to multiple kinematical solutions, difficulties arise when disentangling the exact decay paths.

The aim of the present measurement is to clarify the decay modes of the known excited states and to investigate the existence of states reported in the literature. Beryllium-6 is the subject of a number of theoretical works and, until recently, few experimental data were available. The energy and width of the ground and first excited states, known from early works [1–5], plus the momentum distribution of the α particles in the center-of-mass frame [6,7] were the only data available to test the theoretical calculations. In a recent work [8], a complete kinematic measurement was performed and the correlation between angular and energy distributions of the breakup particles originating from the ground state of ^{6}Be were compared to three-body calculations.

The ground- and first excited-state width and location were satisfactorily interpreted in the past using alternately two- and three-body channels in various models [9–14]. Three states were identified in the $E_{x} \approx 23$ MeV region using ^{3}He + ^{3}He radiative capture [15] and elastic scattering [16]. Inconsistency appears between the latter two works, as pointed out in [17], probably owing to potential interferences in ion-ion scattering reactions observed through elastic scattering measurements but not in radiative capture reaction studies. A number of papers have reported evidence of other states but none of them have been clearly confirmed. A state located around $E_{x} \approx$ 3.0–3.5 MeV has been suggested in a number of references [2,18–20] and predicted in Refs. [21] and [22] but, thus far, never confirmed. An early paper [23] reported about 10 narrow states that, later, were found to be artifacts. Two other states, at $E_{x} = 9.6$ and 18 MeV, were recently reported in Refs. [24] and [17] but still need to be better characterized.

In the present work, results of sequential and three-body resonance calculations are compared to new complete kinematic experimental data for the 0^{+} and 2^{+} states. The sequential decay channels are treated in terms of penetrabilities through the Coulomb/centrifugal barriers folded with the Lorentzian shape of the intermediate resonances. The resulting energy profiles are shown in Fig. 1. Three-body calculations are based on the formalism detailed in Refs. [14,25,26]. After a description of the decay modes of ^{6}Be and theoretical considerations in Sec. II, the experimental procedure is detailed in Sec. III, followed by the experimental results in Sec. IV. The interpretation and comparison between simulated and experimental data are presented in Sec. V, followed by a conclusion.

II. THEORETICAL BACKGROUND

In a number of references, ^{6}Be decay was interpreted in terms of the three-body cluster model using two-body R matrix and various three-body resonance calculations. Two references agree that the decay width of ^{6}Be^{2+} is ≈20% [6] and ≈15% [12] for the diproton channel. In the present work the two approaches for two-body sequential decays and three-body calculations are compared separately.

*papka@tlabs.ac.za; Present address: Department of Physics, University of Stellenbosch, Private Bag X1, 7601 Matieland, South Africa.

†Present address: INFN Sezione di Pisa, Largo Pontecorvo 3, I-56127 Pisa, Italy.

‡Present address: Department of Physics, University of Stellenbosch, Private Bag X1, 7601 Matieland, South Africa.

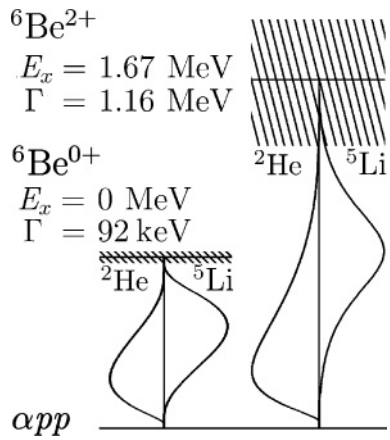

FIG. 1. Relative energy profiles of ^{2}He-^{4}He and ^{5}Li-p calculated for the decay of the ground and first excited states of ^{6}Be.

A. Sequential decay paths

To simulate the sequential decay, the profile of the relative energy between particles must be calculated considering the $^6Be^{0+,2+} \rightarrow {}^2He^{0+} + {}^4He^{0+}$ and $^6Be^{0+,2+} \rightarrow {}^5Li^{3/2-} + p^{1/2+}$ channels. The penetrabilities through the Coulomb plus centrifugal barriers and the Lorentzian shape of the initial and intermediate resonances are folded together. The calculation of these profiles was carried out considering the relative angular momentum deduced from the spin and parity of the initial, intermediate, and final states.

The angles between directions in the two-step decay, represented by θ_1 and θ_2 in Fig. 2, are sensitive to the spin and parity of the parent and daughter nuclei. The expression of the angular distribution in the multistep decay is introduced in the simulations following Eq. (1).

$$W(\theta) = \sum_{\nu} A_\nu P_\nu(\cos\theta). \tag{1}$$

A_ν are the coefficients of the Legendre polynomial series calculated following the Biedenharn and Rose formalism [27].

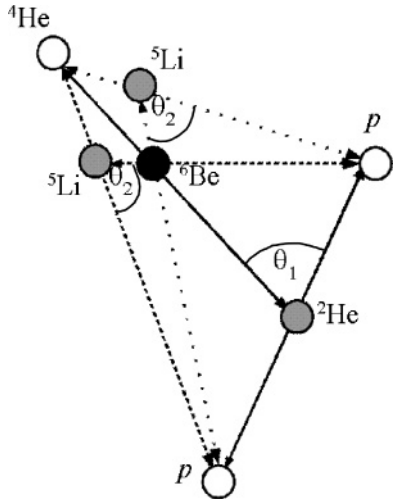

FIG. 2. Diagram of sequential decays and three-body breakup of ^{6}Be.

TABLE I. Details of the sequential decay of $^6Be^{2+}$. The resulting parameters for the Legendre polynomial are $A_0 = 0.714$ and $A_2 = -0.143$ for $^6Be^{2+} \rightarrow {}^5Li^{3/2-} + p^{1/2+}$.

Decay channel	j_1	j	j_2	l_1	l_2	ν_{max}
$^6Be^{2+} \rightarrow {}^2He^{0+} + {}^4He^{0+}$	2	0	1/2 ± 1/2	2	0	0
$^6Be^{2+} \rightarrow {}^5Li^{3/2-} + p^{1/2+}$	2 ± 1/2	3/2	1/2	1	1	2

The details of the two sequential breakup paths are given in Table I. The angular correlation in the two possible sequential decays is expected to be isotropic considering the ^{6}Be ground state, $J^\pi = 0^+$. For the first excited state, owing to the nonzero spin of the parent and daughter resonances, the angular distribution is expected to be anisotropic in the ^{5}Li + p decay channel. The parameters of the Legendre polynomials are calculated to be $A_0 = 0.714$ and $A_2 = -0.143$ according to the values reported in Table I. In the diproton emission, ^{2}He is assumed to be emitted in a pure s wave, therefore the angular distribution in the decay chain is expected to be isotropic. The two-body decays were simulated separately to define the difference between the individual channels.

In all figures, only the θ_1 angular distribution, relative to the ^{6}Be $\rightarrow$ ^{2}He + ^{4}He decay, is shown. Regarding the simulation of the ^{5}Li + p decay path, θ_1 results from the mis-reconstruction of ^{6}Be $\rightarrow$ ^{2}He + ^{4}He. In the case of successive proton emission, θ_1 is sensitive to the θ_2 angular distribution and also to the momentum distribution of the protons.

B. Three-body formalism

Although three-body unbound resonances involve a small number of particles, they pose considerable theoretical challenges owing to their continuum structure. In a first approximation, they can be treated considering the two-body configurations within the resonance. This is the principle of R-matrix formalism used extensively to study two-body systems. Considering ^{6}Be, R-matrix techniques were used in Ref. [12] to calculate the two-proton decay width. Descouvemont *et al.* extended the R-matrix formalism to three-body resonances in ^{6}Be using the hyperspherical harmonic method [13]. The Jacobi coordinates are reduced to five angles and one hyperradius and the long-range interaction is treated through the Lagrange Mesh techniques. The hyperspherical harmonic method was used recently in Ref. [8] to calculate the correlation between the energy and the angular distributions of the breakup particles.

Complete three-body calculations can be treated by means of a many-body Hamiltonian. In the case of unbound states this task rapidly reaches the limits of any actual computation capacity. To overcome this problem, the complex scaling method was developed [28,29] to treat the wave functions expressed in terms of Faddeev equations, initially developed for scattering problems [30]. The functions are rotated in the complex coordinate for each Jacobi coordinate and the problem of unbound states is treated in the same way as the case of bound-state resonances. This method has been used in several studies [10,14,25,31] to calculate the energy and

width of the ^{6}Be states. In Refs. [14,25,26] more information, such as the momentum and position of the breakup particles, is calculated. The energy and width of the ground and first excited states of $A = 6$ isobaric nuclei are generally well reproduced in the aforementioned references, but concerning ^{6}Be, discrepancies arise mainly with the position and width of the 2^+ state.

In the following we include theoretical three-body calculations based on the complex-scaled hyperspherical adiabatic expansion method [14,25,26]. The appropriate coordinates are the hyperradius and five generalized hyperangles. The eigenfunctions of the angular part of the Hamiltonian form the basis to expand the total wave function. Short-range and Coulomb potentials are included. The information on the three-body decay is contained in the large-distance part of the wave function, which must therefore be accurately computed. The integration of the absolute-squared wave function over the hyperangles describing the directions of the momenta gives the single-particle energy distribution. This is performed using Monte Carlo integration. We generate randomly a large number of events, each consisting of three four-momenta relative to the three decaying fragments. The sum of their center-of-mass energies must equal the resonance energy. The weight of each set of momenta is the absolute-squared wave function computed for those momenta. A file was written with 2×10^6 calculated events, where the momentum and angle of every particle are recorded together with a probability weight. Three-body calculations contain all possible combinations of sub-two-body resonances and treat the possible interference between the possible decay modes.

C. Simulations

Monte Carlo simulations were performed with the ROOT [32]-based code *SimSort*. A basic description of this code is given elsewhere [33,34] and more features are implemented in this version. *SimSort* is initially a code for data analysis of complex experimental arrangements comprising coincident measurement of neutrons, γ rays, and charged particles. The code includes numerous packages for kinematic reconstruction, energy loss corrections, and Doppler correction. The experimental setup is defined for data analysis purposes through configuration files of position, geometry, and calibration parameters for each detector channel. The dimension, geometry, gains, and threshold are identical for both simulation and analysis. In this way, precise simulations are performed taking into account the finer details of the experimental setup.

The simulation part of *SimSort* was designed to anticipate the response of the experimental setup. The parameters of the nuclear reaction—in essence, the reaction together with the decay mode and the states of the nuclei— are defined in an input file. Specific parameters like the angular distribution in the decay can also be defined by the user following the formalism detailed earlier [27]. Straightforward reactions can be simulated with a certain ease to optimize an experimental setup.

Regarding precise simulations, *SimSort* is coupled to a number of nuclear model codes. The general idea is to prepare an event in the center-of-mass frame, incorporating the relevant formalism, and to convert it into the laboratory frame through a comprehensive description of the experimental setup. The characterization of unbound states, with reasonably high excitation energy, is relatively straightforward. Regarding cluster-state decays, the Lorentzian width of the states, the angular distribution of the particles, and the decay mode are defined by the user. A successful investigation of the Borromean ^{9}Be nucleus, using the *SimSort* code, is reported in Ref. [34]. Simulation of low-lying states is somewhat more complex owing to the phase-space restriction. If necessary, the penetrability is calculated using Coulomb and centrifugal barriers within the code to anticipate the distortion of the Lorentzian distribution of low-lying states. Empirical or calculated profiles can be predefined and used to generate energy or angular distributions of the decay. This has the advantage of reducing the computing time and allowing the use of experimental data.

The output event file of the three-body calculations, described in the previous section, contains the details of each decay, namely, the momentum distribution and angular correlation of every particle in the center-of-mass frame. *SimSort* processes this event file to compare the calculations to the experimental data properly.

III. MEASUREMENT

A. Experimental method and analysis

An experiment was performed at iThemba LABS, Cape Town, using the ^{6}Li(^{3}He,^{3}H)^{6}Be charge-exchange reaction at a beam energy of $E_{\rm lab} = 50$ MeV. A 5 mg/cm^2 target was made with isotopically enriched material, ^{6}Li $> 95\%$, and kept under inert atmosphere and vacuum during processing and storage to maintain a low level of oxidation [35].

The experimental setup was optimized to detect the three breakup particles, $\alpha - p - p$, plus the recoiling triton with a large acceptance detector arrangement. The four particles were detected in coincidence to measure the correlation between all particles with two double-sided silicon strip detectors (DSSSD). The DSSSDs (50×50 mm^2, 300 μm thick) were placed at a distance of $d = 7$ cm from the target on opposite sides of the beam axis as shown in Fig. 3. The angle from

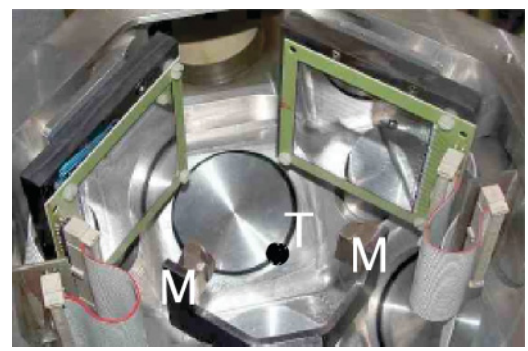

FIG. 3. (Color online) View of the telescopes pointing at the target (T) indicated by a bullet. The two magnets (M), placed on the magnetic arm, are used to deflect electrons of up to 10 keV away from the detectors.

the center of the detectors, with respect to the beam axis, was $\theta_{\rm lab} = 45^\circ$ and the solid angle per detector $\Omega \approx 1$ sr. Each silicon detector was backed with a 60×60 mm^2 CsI(Tl) quadrant, subdivided into 30×30 mm^2 crystals equipped with an individual silicon PIN diode, for E-Δ-E particle identification. The thickness of the CsI(Tl) was 3 mm. For silicon detectors, the punch-through energy for ^{3}H is $\Delta E \approx 10$ MeV, for protons $\Delta E \approx 6$ MeV, while the α particles were identified for an energy deposition of $E_\alpha = 10$–25 MeV and no energy in the corresponding CsI(Tl) element. The scintillators were used for α particles as an offline veto. The total thickness of the telescopes was sufficient to stop protons with energy $E < 25$ MeV, tritons with $E < 40$ MeV, and α particles with $E < 100$ MeV, which was enough to measure the total energy of the ^{6}Be breakup particles populated with a beam energy of $E_{\rm lab} = 50$ MeV.

Owing to the nonlinear response of the CsI(Tl) scintillators, the total energy of the particles was deduced from the energy loss measured in the silicon detectors. The thickness of the silicon had to be corrected event by event according to the incident angle of the particle relative to the center of the detector. The relatively short distance between the target and the detector induces a 10% increase in the effective thickness in the corners compared to the center.

Three particles, at most, were detected per DSSSD, with the condition of three distinct frontside and three distinct backside strips in coincidence to validate an event. The azimuthal angle ϕ between ^{6}Be and ^{3}H, populated in the binary reaction, is selected for $\phi = 180^\circ \pm 5^\circ$. Fourfold events are validated when one α particle, two protons, and one triton are identified with a 2-MeV window condition on the total final-state kinetic energy (TKE) peak $E_{\rm TKE} = E_{\rm lab} - Q = 46.9 \pm 1$ MeV.

Lithium-7 contamination in the enriched material is known to be ≈5%. A run was performed with a natural lithium target (containing ≈92.5% ^{7}Li), with a thickness comparable to that of the enriched target, to subtract a possible contribution from this contaminant. The spectrum obtained using identical sorting conditions is essentially blank and the few events probably result from the natural abundance of ^{6}Li ≈ 7.5%. It is concluded that the contribution from ^{7}Li contamination in the ^{6}Li target is negligible.

The target was relatively thick, ≈5 mg/cm^2, resulting in substantial energy loss of the outgoing particles. Consequently, the TKE peak, being the energy sum of the four detected particles, is broadened and shifted to a lower energy compared to its expected value as shown in Fig. 4 (dotted line). The lowest-energy part of the TKE peak is assigned to interaction points located close to the side of the target facing the beam, while the highest-energy part corresponds to interactions on the downstream side of the target. The thickness of the target material, seen by the particles, is calculated using the interaction point, deduced from the TKE measurement, the thickness of the target, and the emission angle deduced from the DSSSD detector position measurement. It is assumed that the direction of the particles is not substantially altered after passing through the target. From SRIM calculations [36], the average dispersion angle for a 2-MeV proton after multiple scattering through a 5 mg/cm^2 target is about $\delta\theta \approx 1.0^\circ$ and $\delta\theta \approx 0.5^\circ$ for 10-MeV α particles. For the sake of consistency, multiple scattering is also applied to simulated data and an identical correction procedure was applied.

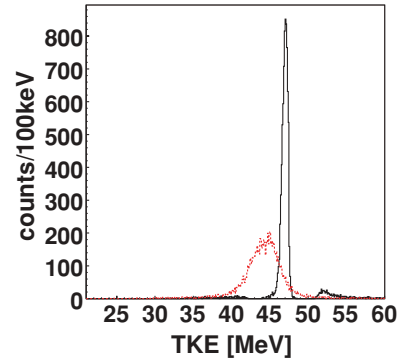

FIG. 4. (Color online) TKE spectra for ^{6}Be ground-state events corrected for energy loss (solid line) and not corrected (dotted line). Selection of ^{6}Be events is performed with a gate on the out-of-plane angle ($\phi = 180^\circ \pm 5^\circ$) and on the excitation energy.

It was checked that the ^{6}Li(^{3}He,^{2}He)αt reaction, with a Q value identical to that of true ^{6}Be events, was not contaminating the ^{6}Be spectrum. Such events were identified in the neutron stripping from ^{3}He, as shown in Fig. 5(a), where the first unbound state at $E_x = 4.63$ MeV is observed. This excitation energy spectrum is obtained from one α particle and one triton detected in coincidence reconstructing the missing diproton. Figure 5(b) shows the experimental two-dimensional (2D) scatterplot of ^{2}He, E versus θ distribution, for ground state to $E_x < 23$ MeV ^{6}Be events. The region where the neutron stripping reaction is expected to appear is indicated between the two solid lines, $E_x > 4.6$ MeV (top line) and $E_x < 15$ MeV (bottom line), in ^{7}Li. Owing to the kinematic selection, very few fourfold events appear in this region but events with an excitation energy in ^{7}Li of $E_x < 15$ MeV

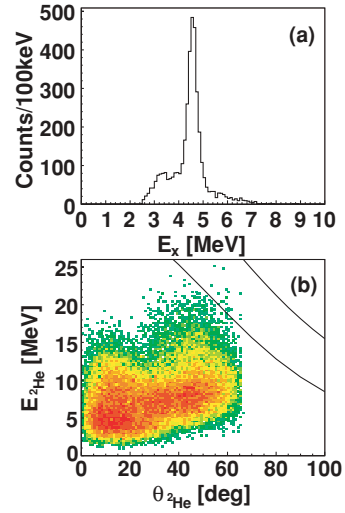

FIG. 5. (Color online) (a) Excitation energy spectrum of ^{7}Li populated in the ^{6}Li(^{3}He,^{2}He) stripping reaction. (b) Scatterplot of E versus θ for reconstructed ^{2}He in the ^{6}Li(^{3}He,^{3}H)^{6}Be* reaction. The locus for ^{2}He populated in the ^{6}Li(^{3}He,^{2}He) reaction is delimited by the solid lines for excitation energy in ^{7}Li, $4.6 < E < 15$ MeV.

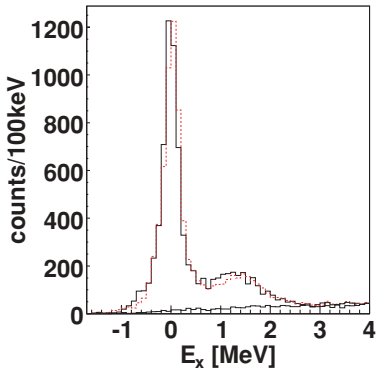

FIG. 6. (Color online) Experimental (solid lines) and simulated (dotted line) excitation energy spectra of the ground and first excited states of ^{6}Be reconstructed from the kinetic energy of the breakup particles in the ^{6}Be center-of-mass frame. A linear background generated randomly is incorporated in the simulation and displayed beneath the true ^{6}Be histograms.

are discarded. However, events corresponding to a very high excitation energy in ^{7}Li cannot be clearly identified owing to the continuum excitation energy expected for $E_x > 15$ MeV. With this detector configuration the $^7\text{Li}^* \rightarrow \alpha + t$ decays, from excitation energy $E_x > 27$ MeV, can fall in the energy region between the ground and the first excited states of ^{6}Be. At such a high excitation energy the decay width of $^7\text{Li} \rightarrow \alpha$-$t$ is not known but it is expected to be rather low owing to the number of open channels at such a high excitation energy. Note also that the maximum energy available at $E_{\text{lab}} = 50$ MeV is $E_x = 30.3$ MeV.

From simulations, the intrinsic resolution of the setup is FWHM = 290 keV at $E_x = 0$ MeV, FWHM = 800 keV in the region of the ^{3}He-^{3}He threshold, and FWHM = 1.6 MeV at $E_x = 20.0$ MeV. The width of the ^{6}Be ground state in Fig. 6 indicates, after the deconvolution of the natural width, an experimental intrinsic resolution of FWHM = 305 keV, which is in good agreement with the simulations.

IV. RESULTS

The excitation energy spectra of Figs. 6 and 7 are reconstructed from the relative energy between the three breakup particles in the ^{6}Be center-of-mass frame selecting true ^{6}Be events. The experimental (solid) and simulated (dotted) spectra in Fig. 6 are populated by the ground and first excited states. The width of the low-lying states is very well reproduced by means of simulation (dotted line), including the natural position and widths of the states; $E_x = 0$ MeV ($\Gamma = 0.092$ MeV) and $E_x = 1.67$ MeV ($\Gamma = 1.16$ MeV). The centroid of the first excited state is shifted to a lower excitation energy compared to its expected value owing to the acceptance of the experimental setup. Because of the very similar kinematics of the three possible breakup channels, the excitation energy spectrum is equally well reproduced with any sequential or three-body simulation. The simulated spectrum in Fig. 6 (dotted) results from the three-body calculation decay channel. A linear background is estimated between 4 MeV, where the 2^+ excited state is expected not to dominate, and

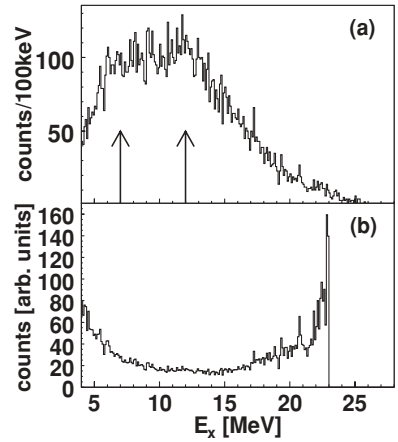

FIG. 7. Excitation energy spectrum of ^{6}Be (a) from experimental data and (b) after correction for efficiency using simulations for the ^{5}Li-p decay channel.

the minimum relative energy between the breakup particles at $E_x = -1.67$ MeV.

The energy spectrum of the $E_x = 4$–23 MeV excitation energy region is depicted in Fig. 7(a). It features a double-humped structure between $E_x = 7$ MeV and $E_x = 12$ MeV, indicated in the figure by the two arrows. An interesting feature lies in the α-p relative energy distribution in the $E_x = 4$–23 MeV excitation energy region of ^{6}Be, as shown in Fig. 8. The peak located at $E_{\alpha p} = 1.97$ MeV (FWHM = 1.23 MeV) is the signature of the ^{5}Li resonance. Approximately 50% of the events result from ^{5}Li decay, and the other half, at higher relative energies, correspond to the first proton emitted with a high ^{5}Li-p relative energy. That the ^{5}Li peak does not arise from the acceptance effect was confirmed by means of simulations. Sequential proton emission was simulated following a uniform random distribution of the kinetic energy, in the center-of-mass frame, between the two protons: in other words, the ^{5}Li resonance was switched off. An increased efficiency is observed in the 0- to 1-MeV region, owing to the detection of the two protons in one telescope, but no such peak appears at $E_{\alpha p} \approx 2$ MeV. Other decay paths, originating from a highly excited ^{9}B, were also simulated including different sequences. The relative α-p spectrum from experimental data

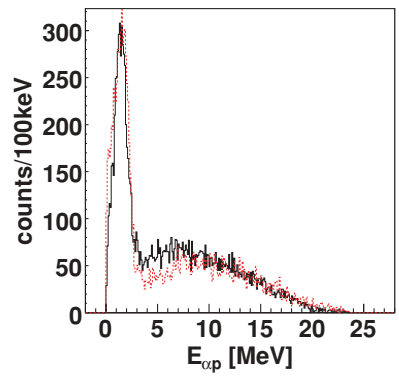

FIG. 8. (Color online) Experimental (solid line) and simulated (dotted line) $E_{\alpha p}$ relative energy spectra corresponding to the decay of ^{6}Be in the $4.0 < E_x < 23$ MeV excitation energy region.

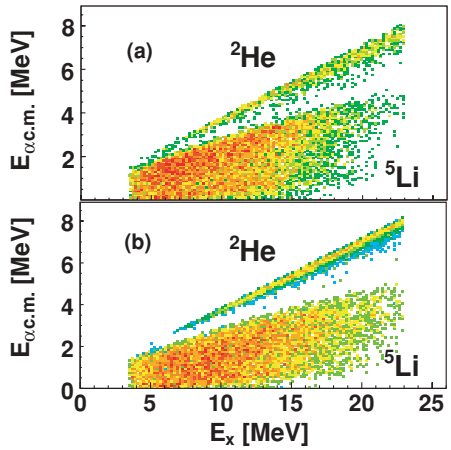

FIG. 9. (Color online) (a) Experimental and (b) simulated $E_{\alpha c.m.}$ energy versus E_x in the ^{6}Be center-of-mass frame for 4 MeV $< E_x <$ 23 MeV. The bottom locus corresponds to ^{5}Li decay, and the top locus to ^{2}He, as indicated in the two spectra.

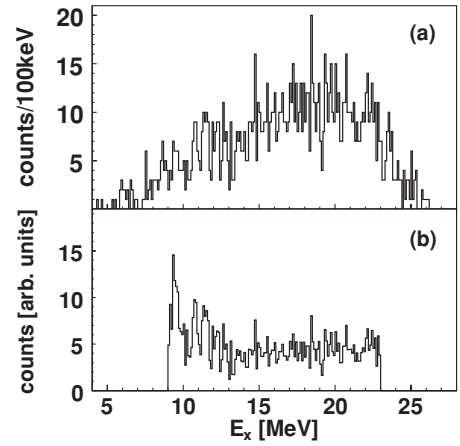

FIG. 10. Excitation energy spectrum of ^{6}Be (a) from experimental data and (b) after correction for efficiency using simulations for the ^{2}He-^{4}He events.

cannot be reproduced with any other alternative path than the ^{5}Li breakup channel.

The structure observed in the excitation energy spectrum in Fig. 7(a) could, in the first instance, be associated with one or two broad states located around $E_x = 7$ and 12 MeV. A careful efficiency correction was performed by means of simulation. A large number of events was generated using the ^{5}Li-p decay channel decaying from a uniform random excitation energy distribution in ^{6}Be between $E_x = 4$ MeV and $E_x = 30$ MeV. The profile of the excitation energy, obtained in this way, reflects the efficiency of the experimental setup. The inverse of this spectrum is then used to correct the experimental energy spectrum. The efficiency correction reveals that the excitation energy distribution is rather continuous, with no clear evidence of states as shown in Fig. 7(b). The double-humped structure has clearly vanished, and only statistical fluctuations remain. The detection efficiency in the excitation energy region $E_x > 20$ MeV is poor, as shown in Fig. 7(b), where the correction factor becomes larger with increasing energy. The corrected spectrum is cut at $E_x =$ 23 MeV as the fluctuations of very low statistics blow at high energy.

Diproton events are clearly identified in the 2D scatterplot in Fig. 9, where the energy of the α particle in the center-of-mass frame is plotted versus the excitation energy of ^{6}Be. The two loci, identified as ^{5}Li-p and ^{2}He-^{4}He in the figure, are very well reproduced with simulations of the individual two-body breakup channels. However, it is impossible to disentangle the ^{2}He-^{4}He decay from the one neutron-stripping reaction where ^{7}Li is produced in the 15- to 25-MeV excitation energy region.

An excitation energy spectrum is shown in Fig. 10 for those events identified as ^{2}He-^{4}He decay in the $E_x > 4$ MeV region. Efficiency correction was applied following the same procedure as described for ^{5}Li-p decay. Simulation of ^{2}He-^{4}He decay was performed using a random uniform excitation energy spectrum of ^{6}Be ranging from $E_x = 4$ to 30 MeV. The experimental spectrum in Fig. 10(a) shows a broad distribution. After efficiency correction the continuous distribution in Fig. 10(b) indicates that the initial broad component arises from acceptance effects.

V. DISCUSSION

Experimental and simulated data are compared in Figs. 11–14. Figures 11 and 14 are constructed in the same way for the 0^+ and 2^+ states, respectively. The energy distributions of α particles and protons, in the ^{6}Be center-of-mass frame, are shown in the left and middle columns in the figures, respectively. The θ_1 angular distribution, reconstructed

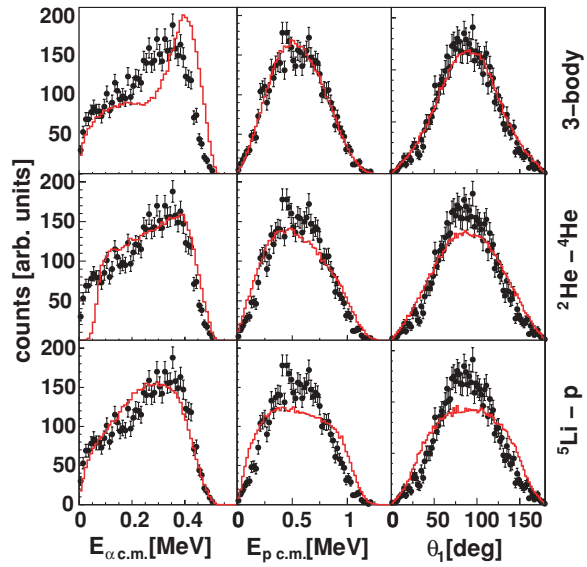

FIG. 11. (Color online) α-particle energy distributions (left column), proton energy distributions (middle column), and θ_1 angular distributions (right column) for measured (filled circles) and simulated (solid line) 0^+ state data. First row: experimental data compared to three-body resonance calculations. Second and third rows: experimental data compared to ^{2}He-^{4}He and ^{5}Li-p sequential decays, respectively.

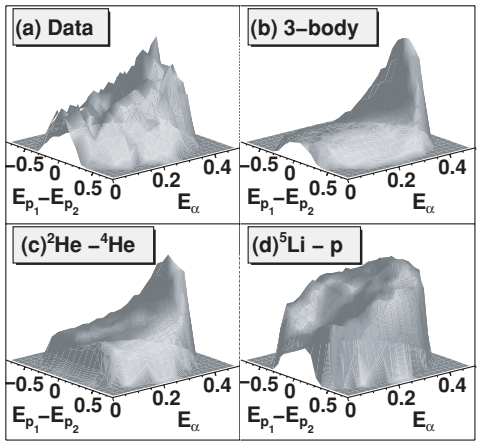

FIG. 12. Zoom on 3D Dalitz plots in Fig. 13 for the 0^+ state. The z axis is a linear projection of the counts and the energy axes are in units of mega–electron volts. The energy difference between the two protons in the center-of-mass frame is projected on the E_{p1}-E_{p2} axis.

considering ^{2}He-^{4}He decay, is depicted in the right column. The ground state is selected for $-0.5 < E_x < 0.5$ MeV. The contaminating events are estimated to count for less than 7% assuming a linear background, as shown in Fig. 6, and the tailing of the 2^+ state at low energy. Compared to the ground state, the 2^+ state is broader and the events of interest are selected with $0.5 < E_x < 2.5$ MeV. Assuming a linear background, displayed in Fig. 6, the contaminating events are estimated to count for about 18% and the contribution of the ground state is neglected in this excitation energy range. The Monte Carlo simulations (solid lines) were performed for approximately 500 000 events to reduce the statistical fluctuations of theoretical distributions.

A. The 0^+ state

The results of three-body simulations are compared to experimental data in the first row in Fig. 11. The simulated proton energy and θ_1 angular distributions are in good agreement with the experimental data. A noticeable difference

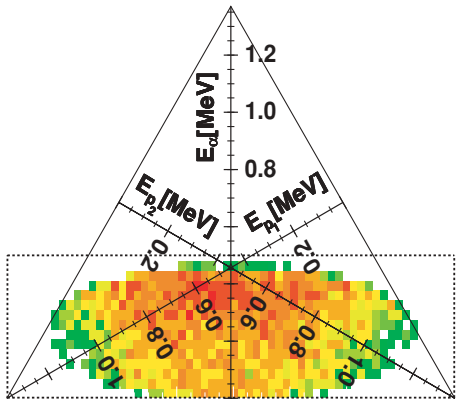

FIG. 13. (Color online) Two-dimensional Dalitz plots for the 0^+ state, with the zoom area (dotted rectangle) for 3D projections shown in Fig. 12.

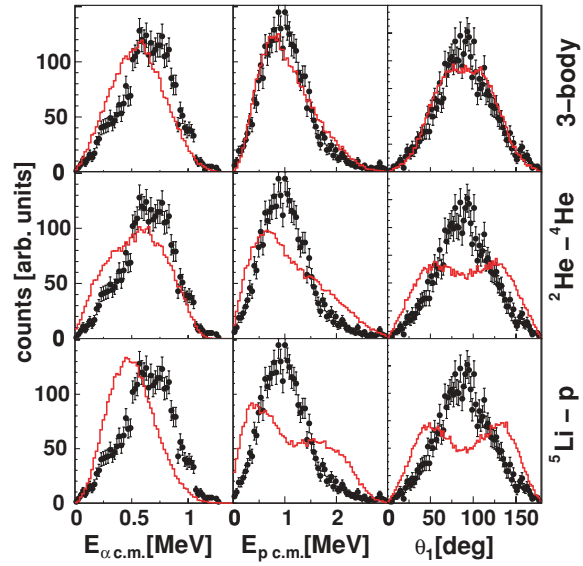

FIG. 14. (Color online) α-particle energy distributions (left column), proton energy distributions (middle column), and θ_1 angular distributions (right column) for measured (filled circles) and simulated (solid lines) 2^+-state data. First row: experimental data are compared to three-body calculations. Second and third rows: experimental data are compared to ^{2}He-^{4}He and ^{5}Li-p, respectively.

lies in the simulated α-particle energy spectrum, where the bump on the high-energy part of the spectrum is narrower and shifted to a higher energy compared to the data. The analysis of the wave function in three-body calculations reveals that the resonance stabilizes for large values of hyperradius ρ where two-body configurations are nonexistent.

The θ_1 and θ_2 angular distributions are expected to be isotropic, considering the two-body decay modes owing to $J^\pi = 0^+$ of the ^{6}Be ground state. The results of the simulation are depicted in the second and third rows in Fig. 11. Using pure ^{2}He-^{4}He decay channel, the agreement between simulated and experimental data is fairly good, although the simulated distributions tend to be generally broader. Moreover, a threshold appears in the low-energy part of the simulated energy spectrum of α particles, which is not consistent with the experimental distribution. The simulated θ_1 profile, using the diproton decay channel, should be isotropic following a sine function. However, the simulation shows that this distribution is peaked around 90°, which is caused by the response of the experimental setup.

The spectra in the third row in Fig. 11 show a strong disagreement between the ^{5}Li-p simulations and the measurement. The simulated energy and angular distributions are much broader than the experimental data, thus it is clear that the decay channel via two sequential protons is very unlikely. As pointed out in Ref. [37], as far as the sequential decay is concerned, ^{2}He-^{4}He should be favored owing to the relative angular momentum $L = 0$ compared to $L = 1$ in the first step decay of ^{5}Li-p. From this analysis, it is concluded that the contribution of the latter decay channel is small.

One-dimensional projections show clearly that the ^{5}Li-p channel can only contribute marginally and it is insufficient to allow the disentanglement of the three-body breakup and pure diproton emission of the 0^+ state. The energy correlation between the three breakup particles is depicted in Figs. 12 and 13, to attempt a clarification of the decay mode of the 0^+ state. For better comparison, the Dalitz plots in Fig. 12 are shown using 3D surface contour projection of the region of interest delimited with a dotted line in the 2D Dalitz plot in Fig. 13. The structure shown for high α momentum in Fig. 12 is observed in all the plots except for ^{5}Li-p decay. The data spread on a 3D scatterplot make the statistics relatively poor and more counts would allow a better comparison between the different spectra. The region $E_{p_1} \approx E_{p_2}$ in the Dalitz plot for ^{2}He-^{4}He is slightly depleted. The same feature tends to appear in the Dalitz plot for the experimental data, but with the present statistics it cannot be clearly confirmed. From this analysis it is not possible to confirm the branching ratio of 15%–30% reported in Refs. [6,8,12] for the ^{2}He-^{4}He decay channel or whether most of the strength decays via three-body breakup as predicted by our three-body calculations. Note that our calculations are in contradiction with the recent results of Grigorenko *et al.* [8]. From their analysis of high-statistics experimental data, enhanced diproton emission is found from the decay of the ^{6}Be ground state.

B. The 2^+ state

Simulated and experimental data for the 2^+ state are shown in Fig. 14. Three-body calculations predict a θ_1 angular distribution slightly broader than the experimental data, but it is in much better agreement compared to the result of sequential decay simulations. The simulation for ^{2}He-^{4}He decay is assumed to proceed exclusively via ^{2}He^{0+} and for ^{5}Li-p via the $3/2^-$ ground state of ^{5}Li. The θ_1 profiles, simulated for the ^{2}He-^{4}He and ^{5}Li-p channels, are characterized by a double-humped structure that is in complete disagreement with the experimental data.

Although the center-of-mass energy distribution for α particles in three-body calculations is slightly shifted to lower energies, by $\approx$100 keV, the overall agreement between simulation and experimental data is much better than for two-body decays. Our three-body calculations predict no contribution from two-body configurations; this is confirmed here through the simulation of the two individual two-body decay channels, which show complete disagreement with the experimental data. Therefore, it is concluded that the three-body configuration dominates the 2^+ state of ^{6}Be.

However, a number of factors can possibly distort the experimental distributions of the breakup particles. Multistep processes were studied for the ^{6}Li(^{3}He,t) reaction at $E_{\rm lab} = 33$ MeV using a polarized ^{3}He beam [38]. The (^{3}He,α)(α,t) and (^{3}He,d)(d,t) reactions were found to contribute substantially at a bombarding energy relatively close to $E_{\rm lab} = 50$ MeV. The population of intermediate resonances in various excited states is likely to interfere with the final resonant states of ^{6}Be. In our calculations it is assumed that the population of ^{6}Be in the 0^+ and 2^+ states occurs via a single-step charge exchange reaction. It is also assumed that the m substates do not contribute, however, they can alter the expected angular distributions in the two-step decay paths.

C. The 4- to 23-MeV excitation energy region

Most of the events in the $E_x > 4$ MeV excitation energy region were shown earlier to proceed via the ^{5}Li resonance. Four-body background can be expected to contribute to the spectrum above the first excited state. Such events originate from low-impact parameter collisions where a typical excitation energy of about 5.5 MeV/A can be obtained in a highly excited ^{9}B "compound nucleus." The four breakup particles are expected to be emitted with no particular correlation between each other, and the formation of ^{5}Li or ^{2}He in such a scenario is very unlikely. The main reason for the low sensitivity to four-body background is the kinematical acceptance of the experimental setup. Events with a relatively equal distribution of p_1-α and p_2-α relative energies, namely, those events corresponding to the breakup of a compound nucleus, have a low probability of entering the two detectors.

The most natural way to populate the ^{5}Li resonance remains, in this system, the charge-exchange reaction where ^{6}Be is produced in a continuum excitation energy region above the 2^+ state. The charge-exchange occurs between a proton of ^{3}He and a neutron of ^{6}Li. Following this direct reaction, the newly formed proton is "knocked out" after the interaction, leaving ^{5}Li nearly as a spectator. It was shown earlier that half of the non-^{2}He events fall under the ^{5}Li peak.

A lower number of ^{6}Be are identified as ^{2}He events but it is not possible to ascertain their origin, as the stripping reaction would mimic the correlation between the two protons. If those events arise from charge exchange reactions, the continuous excitation energy spectrum obtained after efficiency correction does not reveal any structure in ^{6}Be. The formation of two-correlated protons can be expected considering the charge-exchange reaction occurring with the neutron of the deuteron constituent of ^{6}Li. Such diproton emission does not indicate a particular decay mode of ^{6}Be but, rather, reflects the structure of ^{6}Li in its α-d configuration.

The analog states of ^{6}He are expected to be observed in ^{6}Be near $E_x = 6$, 14, and 16 MeV (Γ between 4 and 12 MeV). A state located at $E_x = 18.0 \pm 1.2$ MeV ($\Gamma = 9.2 \pm 1.2$ MeV) is reported to decay via ^{3}He-^{3}He in Ref. [17]. In this reference, the recoils, produced in the charge-exchange reaction ^{6}Li(^{3}He,^{3}H) at 450 MeV were detected at $\theta_{\rm lab} = 0^\circ$. The authors claim that the condition favored a population of a low spin resonance $L = 1$. There is no evidence of αpp decay of these states, mostly owing to their large natural width. The continuous distribution above the 2^+ state could be an admixture of many broad states.

There is no evidence of hypothetical narrower states, as, for example, at $E_x \approx 3.0$–3.5 MeV suggested in Refs. [2,18–20]. A state at $E_x = 9.6$ MeV was recently reported in Ref. [24] using the ^{2}H(^{8}B,^{6}Be)^{4}He reaction. The width of this state is not given, but on the basis of their excitation energy spectrum, the author suggests that it is relatively narrow.

This state is presently not observed in the ^{5}Li-p channel and the statistics are too low to make a conclusion about the ^{2}He-^{4}He channel.

VI. CONCLUSION

No clear indication of any states was found in the 1.67- to 23-MeV excitation energy region. The analog states of ^{6}He are expected to be broader in ^{6}Be owing to the Coulomb repulsion among the three charged particles. Decays through ^{2}He-^{4}He and ^{5}Li-p are observed with a high excitation energy. It is suggested here that the continuum is populated via the ^{6}Li(^{3}He,^{3}H)^{5}Li-p charge-exchange reaction or is an admixture of very broad states. The present data show an enhancement of ^{5}Li-p decay in the 20- to 23-MeV excitation energy region, possibly caused by the 23-, 26-, and 27-MeV states observed in the (^{3}He,^{3}He) reaction [15,16]. Despite the fact that the decay via ^{2}He is observed at a high excitation energy, the kinematics does not allow us to distinguish those events from the ^{6}Li(^{3}He,^{2}He)αt stripping reaction.

This work is the first measurement of the momentum and angular distributions among the three breakup particles of the first excited state of ^{6}Be. The data set collected using the ^{6}Li(^{3}He,^{3}H)^{6}Be reaction was interpreted by means of a three-body cluster model and sequential decay calculations. Comparisons between experimental and simulated data show that ^{6}Be^{2+} has a clear three-body cluster structure. The results are less conclusive concerning the ground state of ^{6}Be. As suggested in the past, decay via ^{5}Li-p is very unlikely. The present three-body calculations predict a pure three-body configuration, which is in contradiction with Ref. [8], where enhanced diproton emission is suggested.

ACKNOWLEDGMENTS

One of us (P.P.) wants to acknowledge F.C. Barker for fruitful discussions and for the calculations of the energy profiles in two-body decay channels. The accelerator staff of iThemba LABS is acknowledged for the good quality ^{3}He beam provided for the measurement. This work has been supported by the Hungarian National Office for Research and Technology (NKTH, Contract Numbers: ZA-7/2006 and ZA-2/2008) and by the National Research Foundation of South Africa (NRF, Contract Numbers GUN2067469 and UID61851). Partial support from the Hungarian Scientific Research Fund, OTKA (Contract Number: K72566) is also acknowledged.

[1] G. F. Bogdanov *et al.*, Sov. J. At. Energy **3**, 987 (1957); At. Energiya **3**, 204 (1957); J. Nucl. Energy **8**, 148 (1958).
[2] F. Ajzenberg-Selove *et al.*, Phys. Rev. **116**, 1521 (1959).
[3] M. Gulyamov, B. V. Rybakov, and V. A. Sidorov, Zh. Eksp. Teor. Fiz. **44**, 1829 (1963); Sov. Phys. JETP **17**, 1230 (1963).
[4] W. Whaling *et al.*, Phys. Rev. **150**, 836 (1966).
[5] J. L. Honsaker *et al.*, Nucl. Phys. A **90**, 545 (1967).
[6] O. V. Bochkarev, A. A. Korsheninnikov, E. A. Kuzmin, I. G. Mukha, A. A. Ogloblin, L. V. Chulkov, and G. B. Yankov, Yad. Fiz. **46**, 12 (1987).
[7] O. V. Bochkarev *et al.*, Nucl. Phys. A **505**, 215 (1989).
[8] L. V. Grigorenko *et al.*, Phys. Lett. B **677**, 30 (2009).
[9] B. V. Danilin, M. V. Zhukov, A. A. Korsheninnikov, L. V. Chulkov, and V. D. Efros, Yad. Fiz. **46**, 427 (1987); Sov. J. Nucl. Phys. **46**, 225 (1987).
[10] A. Csótó, Phys. Rev. C **49**, 3035 (1994).
[11] L. V. Grigorenko, R. C. Johnson, I. G. Mukha, I. J. Thompson, and M. V. Zhukov, Phys. Rev. Lett. **85**, 22 (2000).
[12] F. C. Barker, Phys. Rev. C **66**, 047603 (2002); Phys. Rev. C **67**, 049902(E) (2003).
[13] P. Descouvemont, E. Tursunov, and D. Baye, Nucl. Phys. A **765**, 370 (2006).
[14] E. Garrido, D. V. Fedorov, H. O. U. Fynbo, and A. S. Jensen, Nucl. Phys. A **781**, 387 (2007).
[15] E. Ventura *et al.*, Nucl. Phys. A **219**, 157 (1974).
[16] R. Vlastou, J. B. A. England, O. Karban, S. Baird, and Y.-W. Lui, Nucl. Phys. A **303**, 368 (1978).
[17] T. Yamagata *et al.*, Phys. Rev. C **71**, 064316 (2005).
[18] P. C. Rogers *et al.*, Phys. Rev. Lett. **17**, 148 (1966).
[19] C. J. Batty *et al.*, Nucl. Phys. A **120**, 297 (1968).
[20] B. Wakefield *et al.*, Nucl. Phys. A **114**, 561 (1968).
[21] H. M. Hofmann and W. Zahn, Nucl. Phys. A **368**, 29 (1981).
[22] J. J. Bevelacqua, Phys. Rev. C **33**, 699 (1986).
[23] C. J. Batty *et al.*, Phys. Lett. **19**, 35 (1965).
[24] V. Guimaraes *et al.*, Nucl. Phys. A **722**, 341c (2003).
[25] E. Garrido, D. V. Fedorov, and A. S. Jensen, Eur. Phys. J. A **25**, 365 (2005).
[26] R. Alvarez-Rodriguez, H. O. U. Fynbo, A. S. Jensen, and E. Garrido, Phys. Rev. Lett. **100**, 192501 (2008).
[27] L. C. Biedenharn and M. E. Rose, Rev. Mod. Phys. **25**, 729 (1953).
[28] Y. K. Ho, Phys. Rep. **99**, 1 (1983).
[29] A. Csótó, Phys. Rev. C **49**, 2244 (1994).
[30] L. D. Faddeev, Sov. Phys. JETP **12**, 1014 (1961).
[31] E. Nielsen, D. V. Fedorov, A. S. Jensen, and E. Garrido, Phys. Rep. **347**, 373 (2001).
[32] R. Brun and F. Rademakers, Nucl. Instrum. Methods Phys. Res. A **389**, 81 (1997).
[33] P. Papka *et al.*, Phys. Rev. C **75**, 045803 (2007).
[34] T. A. D. Brown *et al.*, Phys. Rev. C **76**, 054605 (2007).
[35] N. Y. Kheswa *et al.*, Nucl. Instrum. Methods A **613**, 389 (2010).
[36] J. F. Ziegler, Nucl. Instrum. Methods B **219**, 1027 (2004); see also [http://www.SRIM.org].
[37] R. G. H. Robertson, S. Martin, W. R. Falk, D. Ingham, and A. Djaloeis, Phys. Rev. Lett. **32**, 1207 (1974).
[38] A. K. Basak, O. Karban, S. Roman, G. C. Morrison, C. O. Blyth, and J. M. Nelson, Nucl. Phys. A **368**, 74 (1981).